A Functional Interaction Between Y674-R685 Region of the SARS-CoV-2 Spike Protein and the Human α7 Nicotinic Receptor

Juan Facundo Chrestia
CONICET: Consejo Nacional de Investigaciones Cientificas y Tecnicas
Ana Sofia Oliveira
University of Bristol
Adrian J. Mulholland
University of Bristol
Timothy Gallagher
University of Bristol
Isabel Bermúdez
Oxford Brookes University
Cecilia Bouzat (inbouzat@criba.edu.ar)
CONICET: Consejo Nacional de Investigaciones Cientificas y Tecnicas

Research Article

Keywords: nicotinic receptor, neurotransmitter receptors, single-channel recordings, patch-clamp, SARS-CoV-2 spike protein.

Posted Date: March 31st, 2022

DOI: https://doi.org/10.21203/rs.3.rs-1416851/v1

Abstract

The α7 nicotinic acetylcholine receptor (nAChR) is present in neuronal and non-neuronal cells and has anti-inflammatory actions. Molecular dynamics simulations suggested that α7 nAChR interacts with a region of the SARS-CoV-2 spike protein (S), and a potential contribution of nAChRs to COVID-19 pathophysiology has been proposed. We applied whole-cell and single-channel recordings to determine whether the Y674-R685 region of the S protein can directly affect α7 nAChR function. The S fragment exerts a dual effect, acting as a low-efficacy agonist and a non-competitive inhibitor. It activates α7 nAChRs, in line with our previous molecular dynamics simulations showing favorable binding of this accessible region of the S protein to the nAChR agonist binding site. However, activation requires the presence of positive allosteric modulators that enhance open probability, indicating very low efficacy. The main effect of the S fragment on α7 nAChR is a negative modulation, which is evidenced by a profound decrease in the durations of channel openings and activation episodes and in the amplitude of macroscopic responses elicited by ACh. Our study identifies a novel functional interaction between α7 nAChR and a region of the S protein, thus providing molecular foundations for exploring the involvement of nAChRs in COVID-19 pathophysiology.

Introduction

The spike (S) protein is a homotrimeric type I fusion glycoprotein found on the surface of the severe acute respiratory syndrome coronavirus 2 (SARS-CoV-2) and is composed of two subunits, S1 and S2 (Fig. 1A; Supplementary Fig. 1) (Casalino et al. 2020). Binding of S1 to the human angiotensin-converting enzyme 2 (ACE2) is essential for the delivery of the viral RNA into the host cell (Yan et al., 2020; Hoffmann et al., 2020), but infectivity is also affected by additional interactions between S1 and the neuropilin 1 receptor (Daly et al., 2020; Cantuti-Castelvetri et al., 2020). The S protein has been suggested to contribute to COVID-19 pathophysiology also through direct or indirect interactions with other proteins, such as nicotinic acetylcholine receptors (nAChRs) (Changeux et al., 2020; Farsalinos et al., 2020; Oliveira et al., 2021), and epithelial sodium channels (Grant and Lester, 2021).

The interactions between the S protein and nAChRs are thought to occur through the C-terminus region of the S1 subunit (Y674-R685 region) (Changeux et al., 2020). This region is an exposed loop that contains a motif that is homologous to a motif of snake neurotoxins, which are antagonists of nAChRs, and to a short region of the ectodomain of the rabies virus glycoprotein (RABv) (Changeux et al., 2020), which has been shown to inhibit ACh-elicited macroscopic currents of α4β2 nAChRs (Hueffer et al., 2017).

We recently examined the possible binding of the Y674-R685 region of the S protein to several nAChRs using molecular dynamics (MD) simulations (Oliveira et al., 2021). These simulations predicted favourable binding of the Y674-R685 region to the agonist binding site of the human α4β2 and α7 nAChRs (Fig. 1B and C) and the muscle-like αβγδ receptor from *Tetronarce californica* (Oliveira et al., 2021). Moreover, analyses of the MD simulations of the complete and fully glycosylated S protein showed that the Y674-R685 region is accessible for binding (Oliveira et al., 2021). Among nAChRs,

binding of Y674-R685 to the α7 subtype is highly relevant to COVID-19 as nicotine, acting through this receptor, may regulate the expression of ACE2 (Russo et al., 2020). Also, activation of α7 nAChR reduces inflammation and tissue damage by downregulating pro-inflammatory cytokines (Wang et al., 2003; Rosas-Ballina et al., 2008; Egea et al., 2015). Thus, potentiation of α7 has emerged as an important strategy for modulating inflammation in different pathological contexts, including acute respiratory distress syndrome (Egea et al., 2015; Pinheiro et al., 2017). Hence, ligands that bind α7 nAChR may affect the SARS-CoV-2 infectivity and the progression of COVID-19. Indeed, recently it has been shown that varenicline, a full agonist at α7 nAChR (Wonnacott, 2014), reduces infectivity and disease progression in a rhesus macaque model (Nau et al., 2021).

Here, we use whole-cell and single-channel patch clamp recordings to determine whether the Y674-R685 region of the SARS-CoV-2 S protein can directly affect the human α7 nAChR function. Our results reveal that this region acts as a very low-efficacy agonist of α7 since it activates the receptor but only in the presence of a potentiator. Additionally, the Y674-R685 fragment allosterically inhibits α7 responses at a wide concentration range. This functional interaction may play a role in infectivity and/or disease progression and provides foundations for further exploring the involvement of nAChRs in COVID-19 pathophysiology.

Materials And Methods

Chemicals.

Acetylcholine (ACh) and 5-Hydroxyindole (5-HI) were purchased from Merck (USA). PNU-120596 (N-(5-Chloro-2,4-dimethoxyphenyl)-N’-(5-methyl-3-isoxazolyl)-urea) was obtained from Tocris Biosciences (Bristol, UK). Stock solutions were prepared in water (ACh, 5-HI) or DMSO (PNU-120596). The fragment of the S protein (S) of SARS-COV-2, called Y674-R685, contains 12 amino acids with the sequence YQTQTNSPRRAR (MW 1477.60). The peptide was synthesized (90% purity) by Designer Bioscience Ltd. (Cambridge UK) and stored as 1 mM stock solutions (in water) at -20°C.

Expression of human α7 in mammalian cells.

BOSC-23 cells, derived from HEK-293 cells (kindly provided by Dr. Sine, Mayo Clinic, USA), were cultured with Dulbecco’s Modified Eagle Medium (DMEM) culture medium (GIBCO, USA) supplemented with 100 µg/mL streptomycin – 100 IU/mL penicillin (Invitrogen, USA), 10% Fetal Bovine Serum (FBS, Internegocios, Argentina). Human α7 cDNA subunit (GenBank accession no X70297.1) was subcloned into the pRBG4 expression vector (Bouzat et al., 1994; Chrestia et al., 2021). BOSC-23 cells were transfected by the calcium phosphate procedure with α7 subunit cDNA together with the α7 chaperones Ric-3 and NACHO cDNAs (Lansdell et al., 2005; Gu et al., 2016). The cDNA ratio was 1:2:1 for α7:Ric-3:NACHO, and the total amount was 4.2 µg/ 35 mm dish. Also, green fluorescence protein (GFP) cDNA plasmid was included to allow the identification of transfected cells (Nielsen et al., 2019; Lasala et al., 2019).

All transfections were carried out for about 8–12 h in DMEM with 10% FBS and terminated by exchanging the medium. Cells were used for experiments two to three days after transfection, at which time maximum functional expression levels were achieved (Andersen et al., 2016; Bouzat et al., 1994; Bouzat et al., 2008).

Single-channel recordings in BOSC-23 cells.

Single channels were recorded in the cell-attached patch configuration at -70 mV (Bouzat et al., 2008). Each patch corresponds to a different cell (n indicates the number of independent experiments). For each condition, at least three different cell transfections from distinct days were performed (N indicates the number of cell transfections).

The bath and pipette solutions contained 142 mM KCl, 5.4 mM NaCl, 1.8 mM $CaCl_2$, 1.7 mM $MgCl_2$ and 10 mM HEPES (pH 7.4). The peptide and 5-HI dissolved in water were added directly to the pipette solution. PNU-120596 in DMSO was added either to the pipette solution or to the dish. The final concentration of DMSO was lower than 0.1% (v/v), which does not affect α7 activation properties (Chrestia et al., 2021).

Single-channel currents were digitized at 5–10 μs intervals and low-pass filtered at a cut-off frequency of 10 kHz using an Axopatch 200B patch-clamp amplifier (Molecular Devices, CA, USA). Analysis was performed with the program TAC (Bruxton Corporation, Seattle, WA, USA) with the Gaussian digital filter at 9 kHz (Final cut-off frequency 6.7 kHz) or at 3 kHz for recordings in the presence of PNU-120596. Events were detected by the half-amplitude threshold criterion (Bouzat et al., 2008).

Open-time histograms were fitted by the sum of exponential functions by maximum likelihood using the program TACFit (Bruxton Corporation, Seattle, WA, USA). The duration of the slowest open component was used for comparisons. Bursts of channel openings were identified as a series of closely separated openings preceded and followed by closings longer than a critical duration, which was taken as the point of intersection between closed components as previously described (Andersen et al., 2013, 2016; Bouzat et al., 2008). For α7 activated by ACh, the critical duration for defining a burst was defined by the intersection between the first and second briefest components in the closed-time histogram (~200–400 μs). For defining bursts in the presence of 5-HI, critical times were selected between the second and third closed components (~1–3 ms) (Bouzat et al., 2008; Andersen et al., 2013, 2016). In the presence of PNU-120596 and ACh, α7 nAChR openings are grouped in bursts, and several bursts form long clusters. Each cluster corresponds to the activation episode of the same receptor molecule. For bursts, the critical time was set at 200–400 μs, and for clusters, the critical time was determined by the point of intersection between the third and fourth closed components (~30–60 ms) (Andersen et al., 2016). The burst and cluster durations were taken from the slowest components of the corresponding histograms (Bouzat et al., 2008; Andersen et al., 2016).

Expression of α7 nAChR in Xenopus laevis **oocytes**.

Adult female *Xenopus laevis* were purchased from *Xenopus* One, MI, USA. *Xenopus* care and housing followed the UK Home Office code of practice guidelines for the species. Stage V and VI *Xenopus* oocytes were prepared as previously described (Minguez-Viñas et al., 2021), and then injected with 2–6 ng of human α7 subunit cDNA into the nucleus in a volume of 23.0 nL, using a Nanoject Automatic Oocyte Injector (Drummond, Broomall, USA). To favour the expression of α7, its cDNA was co-injected with chaperone NACHO cDNA (GenBank accession no BC050273.1) at a ratio of 1 α7: 0.01 NACHO (Gu et al., 2016; Nielsen et al., 2018). Injected oocytes were incubated until use at 18ºC in a solution (OR2) containing 82 mM NaCl, 2 mM KCl, 2 mM $MgCl_2$, 5 mM HEPES; pH 7.5, supplemented with 0.1 mg/mL streptomycin, 1000 U/mL Penicillin and 100 µg/mL amikacin. Oocytes were used for electrophysiological recordings one to two days after injection (Nielsen et al., 2018; Minguez-Viñas et al., 2021).

Electrophysiological recordings in Xenopus laevis **oocytes.**

Oocytes were impaled with two electrodes filled with 3 M KCl, and the voltage-clamp was maintained at -60 mV throughout the experiment. All recordings were performed at 18°C, and cells were perfused continuously with OR2 solution at pH 7.4. Currents were recorded using an automated platform equipped with standard two electrode voltage-clamp configuration (HiClamp; Multi Channel Systems, Reutlingen, Germany). This system differs from standard electrophysiology and other automated platforms because, instead of applying the compound in the perfusion, the oocyte is moved into a well from a 96-well microtiter plate containing 230 µl of the desired solution, as previously described (Minguez-Viñas et al., 2021). Experiments were carried out only if the resting potential of the impaled oocytes was greater than − 10 mV and the total holding current less than 0.2 µA.

The ability of fragment Y674-R685 to evoke current responses in *Xenopus* oocytes expressing α7 nAChR was examined at a range of concentrations (1 pM-10 µM) along with control EC_{50} (100 µM) ACh-evoked responses from the same cells. Compounds were applied for 20 s and the washout period was 5 min. For experiments that assessed the effects PNU-120596 on the ability of fragment Y674-R685 to activate α7 nAChRs, oocytes displaying maximal ACh current amplitudes of 15–20 µA were used. Our limit of detection for α7 receptor-mediated activity is 0.05–0.08% (10–20 nA of current) of the maximal responses elicited by 1 mM ACh.

To obtain concentration response data for the inhibitory effects of Y674-R685 on α7 nAChRs, a range of concentrations of the fragment (0.1 nM to 30 µM) were co-applied with ACh EC_{50} (100 µM). The peaks of the current responses obtained in this manner were then normalised to the peak of the responses elicited by ACh alone. The effects of the fragment on the ACh concentration response curve (CRC) were assessed by determining the ACh CRC in the absence and presence of 1 µM Y674-R685. The peak of the ACh responses were normalised to the responses elicited by 1 mM ACh. For both set of studies, the normalised data were fit with the Hill equation using GraphPad software version 5, as previously described (Minguez-Viñas et al., 2021). Data are expressed as means ± SEM from 5–6 oocytes obtained from at least three different batches of oocytes (N).

Data were filtered at 10 Hz, captured at 100 Hz using proprietary data acquisition software running under Matlab (Mathworks Inc., Natick, MA).

Statistical analysis.

Single-channel data are presented as mean ± SD. Data sets that passed the Shapiro-Wilk test for normality and the Levene Median test for equal variance were analyzed using two-tailed Student's t-test for pairwise comparisons or Mann-Whitney rank sum test with SigmaPlot 12.0 (Sysat Software, Inc.). Statistically significant differences between two groups of data were established at p values < 0.05. For each condition, n indicates the number of independent experiments, each from different cell patches, and N, the number of cell transfections, each from different days and cell batches.

Results

α7 nAChR activation by the Y674-R685 fragment from the SARS-CoV-2 S protein in the presence of potentiators.

Our previous MD simulations of the complex formed between the α7 nAChR and the Y674-R685 fragment from the SARS-CoV-2 S protein suggested the potential of the Y674-R685 region to interact with conserved aromatic residues within the binding pocket of the receptor (Fig. 1C) (Oliveira et al., 2021). To establish unequivocally the existence of molecular functional interactions between this region of SARS-CoV-2 S protein and the human α7 nAChR, we evaluated whether the synthetic fragment could elicit macroscopic and high-resolution single-channel currents.

The macroscopic responses of the human α7 nAChR expressed in *Xenopus* oocytes to the applications of the Y674-R685 fragment at a range of concentrations (1 pM-10 μM) were examined along with control ACh-evoked responses from the same cells (Fig. 2A). As shown in the figure, Y674-R685 did not elicit detectable currents in contrast to the robust responses elicited by 100 μM ACh. After 5 min wash, receptors remained responsive to subsequent control applications of ACh (Fig. 2A).

Single-channel currents from cell-attached patches from BOSC-23 cells expressing human α7 nAChR were also recorded, thus allowing for more detailed mechanistic information. Recordings were carried out in parallel with control experiments with ACh as the agonist to confirm the presence of functional α7 nAChRs in the same batch of cells. ACh (10–100 μM) evoked isolated brief openings or less often short bursts composed of a few openings in quick succession, which correspond to activation of the same receptor molecule (Bouzat et al., 2008; Andersen et al., 2013; Nielsen et al., 2019; Chrestia et al., 2021) (Fig. 2B). In contrast, channel activity was not detected at a range of Y674-R685 concentrations in a total of 21 patches from different cell transfections (1 pM, n = 3; 1 nM, n = 3; 1 μM, n = 8; 10 μM, n = 3; 100 μM, n = 4) (Fig. 2B).

Given that α7 nAChR activation in the presence of ACh occurs with low open probability as very brief opening events (Fig. 2B), we sought to amplify this effect using a potentiator. PNU-120596, a type II

positive allosteric modulator (PAM), has been extensively used as a tool in α7 nAChR functional studies due to its ability to increase the probability of agonist-elicited channel opening and open-channel durations and to reduce desensitization (daCosta et al., 2011). We, therefore, examined whether Y674-R685 elicits α7 channel activity in the presence of PNU-120596. Note that by itself, PNU-120596 cannot induce channel activation (Hurst et al., 2005).

The macroscopic currents elicited by 1 μM Y674-R685 in the presence of 10 μM PNU-120596 were recorded. Under these conditions, small currents in the low nA order were detected in 30% of the oocytes tested whereas neither Y674-R685 nor PNU-120596 on their own elicited currents (n = 15, N = 3) (Fig. 3A).

To gain more insights into how Y674-R685 activates α7 nAChRs in the presence of PNU-120596, we explored its effects at the single-channel level. ACh-elicited activity in the presence of 1 μM PNU-120596 is profoundly different to that in its absence (Fig. 3B). Instead of the brief isolated openings, channel activity shows long periods of high-frequency openings, named clusters, with a mean duration of about 1–3 s and an amplitude of 10 pA (-70 mV). A cluster corresponds to the activation episode of the same receptor that recovers from desensitization and oscillates between open and closed states before reaching again the more stable non-conducting desensitized state (daCosta et al., 2011). Clusters are composed of bursts with mean durations of ~ 200–500 ms, which comprise successive openings separated by very brief closings (Figs. 3B and 4) (daCosta et al., 2011; Andersen et al., 2016).

In the presence of 1 μM PNU-120596, Y674-R685 was capable of eliciting channel activity at a wide range of concentrations (1 pM to 10 μM), indicating that this region of the S protein can activate α7 nAChRs (Fig. 3B). Since the frequency of channels is variable among patches due to variations in receptor expression levels, parallel control recordings in the presence of ACh were made. When ACh and PNU-120596 were co-applied, > 98% of patches showed channel activity (active patches), and the long-duration clusters described above appeared at high frequency as reported before (Lasala et al., 2019) (Fig. 3B). In the presence of PNU-120596 and Y674-R685, the percentage of active patches was lower than in the presence of ACh: 65% (n = 23, N = 4; 1 pM Y674-R685), 40% (n = 15, N = 4; 1 nM Y674-R685), 67% (n = 15, N = 4; 1 μM Y674-R685), and 62% (n = 13, N = 3; 10 μM Y674-R685). Also, channel activity evoked by Y674-R685 was much more infrequent and interspaced by long silent periods when compared to that evoked by ACh (Fig. 3B). It is important to note that this type of experiments does not allow for a precise comparison of channel frequency since this parameter may be affected by the variability in the number of receptors in each patch. Nevertheless, at 1 pM Y674-R685, the frequency of channel activation episodes was very low; albeit the active patches showed long clusters resembling those elicited by ACh and PNU-120596 (Figs. 3B and 4).

The increase in Y674-R685 concentration resulted in profound changes in the channel activity pattern, as clearly illustrated in the recordings shown in Fig. 3B. The frequency of opening events appeared to increase, but the duration of the openings and the activation episodes were reduced with increasing concentrations. The typical long-duration clusters were completely absent at Y674-R685 concentrations

higher than 1 μM, at which activation occurred mainly as isolated openings or in short bursts (Fig. 3B and 4).

To define the properties of the activation episodes elicited by the Y674-R685 fragment at different concentrations, the mean durations of openings, bursts, and clusters in the presence of PNU-120596 were determined (Fig. 4). At 1 pM Y674-R685, the mean durations of the longest openings, bursts and clusters were 141 ± 59 ms, 417 ± 113 ms, and 2330 ± 673 ms, respectively (n = 3). These values were similar to those determined in the presence of 10 μM ACh: 148 ± 12 ms for the slowest open component (p = 0.859, n = 3), 550 ± 38 ms for bursts (p = 0.125, n = 3), and 3048 ± 516 ms for clusters (p = 0.217, n = 3), and also comparable to those reported before for 100 μM ACh and 1 μM PNU-120596 (daCosta et al., 2011; Andersen et al., 2016). Although the mean durations of clusters were similar at 10 μM ACh and 1 pM Y674-R685, the relative area of the components corresponding to clusters in the histogram was smaller when Y674-R685 was the agonist (relative areas were for ACh = 0.44 ± 0.09 and for Y674-R685 = 0.21 ± 0.08; p = 0.0264) (Fig. 4), indicating a reduction in the frequency of the long activation episodes.

With the increase of Y674-R685 concentration, dwell time distributions for open, bursts and clusters were shifted to briefer durations. The slowest component of each histogram became progressively briefer with increasing Y674-R685 concentrations (Fig. 4). The mean durations were 48.2 ± 13.6 ms (1 μM, n = 3) and 14.5 ± 4.3 ms (10 μM, n = 4) for openings; 70.2 ± 19.7 ms (1 μM, n = 3) and 20.7 ± 8.0 ms (10 μM, n = 4) for bursts; and 104.2 ± 41.6 ms (1 μM, n = 3) and 29.9 ± 14.8 ms (10 μM, n = 4) for clusters. Mean values were statistically significantly different to those determined in the presence of 10 μM ACh and 1 μM PNU-120596 (p = 0.000665 and p = 0.00000431 for open; p = 0.0000403 and p = 0.00000106 for burst; p = 0.000597 and p = 0.0000681 for cluster, for 1 and 10 μM Y674-R685, respectively). At high Y674-R685 concentrations (e.g., 10 μM), the mean open duration was similar to the mean burst and cluster durations (Fig. 4), indicating that openings occurred mostly in isolation and confirming the lack of the typical long-duration clusters corresponding to potentiated α7 nAChR responses.

To further confirm that channel activation can be elicited by Y674-R685 in the presence of PNU-120596 but not in its absence a different strategy was followed. Single-channel recordings in the presence of different concentrations of the Y674-R685 fragment (1 μM and 10 μM) were performed. Again, no channel activity was detected in all patches (n = 9, N = 2). However, the addition of 1 μM PNU-120596 to the dish during the course of the recording resulted in the appearance of single-channel activity in most of the silent patches (83.3% and 100% for 1 μM (n = 6) and 10 μM Y674-R685 (n = 3), respectively) (Fig. 5). Since this strategy allows comparison of both conditions (with and without PNU-120596) in the same patch, it confirms that activation by Y674-R685 requires the PAM. The same strategy applied using ACh as the agonist showed that the typical brief isolated openings are replaced by long-duration clusters after addition of PNU-120596 (Fig. 5, daCosta et al., 2011). The frequency of opening events was markedly lower, and the durations were briefer at 10 μM Y674-R685 with respect to the recordings with ACh (Fig. 5).

Together, these results confirm that Y674-R685 functionally interacts with the α7 nAChR. They also show that Y674-R685 acts as a very low-efficacy agonist since channel opening requires the presence of PNU-120596 and occurs with low probability, and that the increase in concentration is accompanied by a decrease in the duration of open channel lifetime and of the activation episodes.

Because PNU-120596 is a highly efficacious type II PAM with the capability of recovering receptors from desensitization, we also tested if Y674-R685 elicited channel activity in the presence of 5-hydroxyindole (5-HI), a type I PAM. This compound induces potentiation with lower efficacy than PNU-120596 and does not recover receptors from desensitization (Zwart et al., 2002; Andersen et al., 2016; Nielsen et al., 2019). In the presence of 2 mM 5-HI, 100 μM ACh elicited prolonged openings and bursts composed of successive openings which lasted about 4 ms (Fig. 6). The histograms showed that the duration of the slowest open component was 4-fold longer (1.28 ± 0.35 ms, n = 37, versus 0.30 ± 0.06 ms, n = 38) and the mean burst duration was 8-fold longer (3.60 ± 1.29 ms, n = 37, versus 0.46 ± 0.12 ms, n = 38) than in the absence of the PAM. Replacing ACh by Y674-R685 (1 pM or 10 μM) revealed α7 channel activity. However, the frequency of opening events was markedly lower when compared to that elicited by ACh; only few events were detected during a 15-min recording period (Fig. 6). At 1 pM Y674-R685, 83.3% of the patches showed α7 channel activity, but the frequency of openings was very low (n = 18, N = 3). We therefore combined all recordings for constructing open and burst duration histograms. The resulting mean open and burst durations were 1.11 ms and 4.25 ms, respectively (Supplementary Fig. 2). At 10 μM Y674-R685, the frequency of channel openings was higher than at 1 pM but still lower than that elicited by ACh. The mean open and burst durations were 0.73 ± 0.07 ms and 0.85 ± 0.13 ms (n = 3), respectively. Both mean durations were statistically significantly briefer than the corresponding ones in the presence of ACh and 2 mM 5-HI ($p = 0.0114$ and 0.005 for mean open and mean burst durations, respectively). Also, the observation that in the presence of 2 mM 5-HI and 10 μM Y674-R685 the mean duration of openings was similar to that of bursts indicates that at high fragment concentrations channel openings occurred mainly as isolated events instead of in quick succession forming activation episodes, as described before for recordings with the type II PAM PNU-120596.

Inhibition of α7 activity by Y674-R685 from S protein

To understand the molecular mechanisms driving the inhibitory effects of Y674-R685 evidenced by the dramatic decrease in open durations, we evaluated Y674-R685 effects on α7 activated by 10 μM ACh (Fig. 7A). Given the very brief open duration of α7 channels, which is close to the time resolution of our system, we included PNU-120596 to better quantify the decrease in open durations.

Whereas in the presence of 1 μM PNU-120596, 10 μM ACh led to an activation pattern composed of long clusters as described above, the inclusion of Y674-R685 produced marked changes in this pattern in a concentration-dependent manner. Y674-R685 produced an inhibitory effect even at a concentration as low as 1 pM (Fig. 7A and Supplementary Table 1). The results showed that the cluster duration was the most sensitive parameter. With respect to the control recordings with ACh and PNU-120596, the presence of 1 pM and 1 nM Y674-R685 reduced the cluster duration 72% and 78%, respectively, and the open

duration 54% and 57%, respectively (Fig. 7A, Supplementary Table 1). As the concentration increased, the inhibition was more evident and at 10 μM Y674-R685, the long durations clusters were absent, and only markedly briefer bursts were detected (Fig. 7A and Supplementary Table 1). At this high concentration, the mean duration of the slowest open component was 9.9 ± 2.6 ms (n = 4), which corresponds to about 7% of the control open duration. Also, the open duration was not different from the mean burst duration (11.2 ± 3.0 ms, n = 4), indicating that most long openings occurred in isolation (Supplementary Table 1). Although clusters were not visually detected, we constructed cluster duration histograms using a critical time for cluster resolution between 10 and 20 ms, which is about 20 to 40-fold times longer than that used for burst-duration histograms. The mean duration of the slowest component of the cluster histogram was 14.1 ± 4.4 ms (n = 4), which was similar to that of bursts, thus confirming the lack of the long-duration activation episodes occurring in potentiated α7 channels in the presence of 10 μM Y674-R685 (Fig. 7A, Supplementary Table 1).

To gain further insight into the mechanism driving the inhibitory effect of Y674-R685 in the presence of ACh and PNU-120596, we compared the pattern of channel activity when methyllycaconitine (MLA), a reversible competitive α7 antagonist (Wonnacott, 2014), was present instead of the S fragment. To better assess the impact of MLA, we used the strategy of filling the tip of the pipette with the buffer solution containing 10 μM ACh and 1 μM PNU-120596 and the shaft with the same solution but including MLA (100 nM). This strategy allowed following in real-time the effects of the antagonist during the recording of ACh-activated channels. While at the beginning of the recording the typical pattern comprising high-frequency channel activity and long duration clusters was observed, channel activity decreased over time and was completely suppressed after about 10–15 min due to the presence of MLA (Supplementary Fig. 3, n = 3). No reduction in the duration of clusters or bursts, as described in the presence of Y674-R685, was detected in the presence of MLA (Supplementary Fig. 3). Thus, the type of inhibition mediated by Y674-R685 differs from that produced by the competitive antagonist.

The results together suggest that the Y674-R685 region of the S protein acts as a non-competitive antagonist of α7. To further confirm this result, we determined the effects of Y674-R685 on the peak current responses evoked by an approximate EC_{50} concentration of ACh (100 μM). Application of Y674-R685 with ACh inhibited peak currents, with an IC_{50} of 1.8 ± 0.8 μM (n = 10), but inhibition was not complete (Fig. 7B). We then investigated whether the observed antagonism was competitive or not. For these studies, 1 μM Y674-R685 was co-applied with increasing concentrations of ACh (0.1–2000 μM) (Fig. 7B). Compared to ACh alone, Y674-R685 co-application affected ACh efficacy, reducing the maximal currents elicited by ACh (Imax) by 30 ± 4% (n = 6) and slightly affecting its potency (EC_{50} = 80 ± 6 μM and 131 ± 92 μM) (n = 6). These results confirm the non-competitive antagonism of ACh responses by Y674-R685.

Discussion

Here, we provide the first molecular evidence of a direct functional interaction between human α7 nAChR and the Y674-R685 region of the SARS-CoV-2 S protein. This interaction, which takes place within the

picomolar to micromolar concentration range, results in a dual effect involving low efficacious agonism and non-competitive antagonism. Our findings agree with our previous MD simulations that revealed a possible interaction between the accessible Y674-R685 region of the SARS-CoV-2 S protein and nAChRs (Oliveira et al., 2021).

α7 is a homomeric nAChR highly expressed in both neuronal and non-neuronal cells, which is emerging as a potential drug target for neurological, neurodegenerative, and inflammatory disorders (Uteshev, 2014; Dineley et al., 2015; Yang et al., 2017). It responds to ACh by opening an intrinsic ion channel permeable to cations, triggering rapid membrane depolarization and calcium influx (Bouzat et al., 2018). α7 activation is unique as it shows the most rapid desensitization and the highest calcium permeability of the family (Fucile, 2004). Here, by taking advantage of the power of single-channel recordings, we provide novel information regarding the molecular functional effects and the underlying mechanisms of the interaction between the α7 nAChR and the Y674-R685 region of the SARS-CoV-2 S protein.

We found that Y674-R685 activates the α7 receptor at picomolar concentrations but with exceptionally low efficacy. The efficacy for activation is so low that only in the presence of PAMs channel activity can be detected, and, even in their presence, the frequency of channel activity induced by the fragment is markedly lower than the one elicited by ACh. In addition, ACh-elicited responses are reduced by the S protein fragment, indicating a dual function as agonist and inhibitor. Given that endogenous α7 PAMs, with the exception of calcium, have not been reported so far, the S protein may physiologically play an inhibitory role at α7. α7 nAChR also mediates metabotropic responses, which include release of calcium from intracellular stores induced by the calcium influx and the triggering of signal transduction pathways (Kabbani et al., 2013; Egea et al., 2015; Guan et al., 2015; Bouzat et al., 2018). This raises important questions regarding how these metabotropic responses are modified by the S protein and their impact on COVID-19 pathophysiology. Interestingly, the neurotoxin-like region in the rabies virus glycoprotein as well as the full length ectodomain of the glycoprotein inhibit macroscopic responses of α4β2 nAChRs in the mid-micromolar range. The fragment also mediates *in vivo* effects in mice and *Caenorhabditis elegans* (Hueffer et al., 2017).

PAMs, which reduce the energy barrier for activation, are emerging as novel therapeutic tools for neurological, neurodegenerative, and inflammatory disorders as they potentiate α7 responses in the presence of an agonist (Changeux and Taly, 2008; Uteshev, 2014; Dineley et al., 2015; Chatzidaki and Millar, 2015). They have been classified as type I PAMs, which enhance agonist-induced macroscopic currents, and type II PAMs, that also delay desensitization and recover receptors from desensitized states (Bertrand and Gopalakrishnan, 2007; Grønlien et al., 2007; Andersen et al., 2016). At the single channel level, PAMs enhance open channel durations and induce activation in episodes in which the channel oscillates between open and closed conformations, thus generating an activity pattern markedly different from the isolated sub millisecond-openings in the absence of PAMs (Andersen et al., 2016). Depending on the type and efficacy of the PAM, the potentiated activation episodes can range from milliseconds (as shown here for 5-HI) to seconds (as demonstrated here for PNU-120596). Despite the marked differences between 5-HI and PNU-120596 regarding their efficacy for potentiation and influence on receptor

desensitization, Y674-R685 activates the α7 nAChR in the presence of both PAMs but not in their absence, indicating its action as a low-efficacy agonist. Also, in the presence of both PAMs, reduction in the duration of the opening events with increasing Y674-R685 concentration is observed, thus supporting the additional role of this fragment as an α7 inhibitor.

At 1 pM Y674-R685, channel activity in the presence of PNU-120596 is markedly infrequent but kinetically indistinguishable from the ACh-elicited one. The open channel lifetime, and the architecture and duration of the activation episodes (clusters) are similar in the presence of ACh or 1 pM Y674-R685. As the Y674-R685 concentration increases, the frequency of opening events increases, but their durations become progressively briefer and long-duration clusters are not detected. This inhibitory effect was confirmed by experiments in which ACh was the agonist, clearly showing a concentration-dependent reduction of open and cluster durations by the Y674-R685 fragment. To determine if this modified channel activity pattern was similar to that observed in the presence of a reversible competitive antagonist, we also explored how MLA affected α7 potentiated channels. The results showed that the type of channel inhibition was completely different, suggesting different mechanisms. The classical pharmacological experiments using dose-response curves from macroscopic current recordings support a mechanism of non-competitive inhibition exerted by the S protein fragment.

The ability to act as a low-efficacy agonist is consistent with data from our MD simulations predicting that Y674-R685 can bind directly to the agonist binding site located in the extracellular domain of the α7 nAChR, leading in some conformations to a semi-capped loop C (Oliveira et al., 2021). Loop C is one of the three loops that form the principal face of the orthosteric binding site (Noviello et al., 2021). Upon agonist binding, loop C closes to cap the agonist, an event associated with priming and channel opening (Mukhtasimova et al., 2009). Loop C capping aids the anchoring of the bound agonist to the orthosteric binding site. It has also been suggested that agonists induce more compact loop conformations, while partial agonists and antagonists produce incomplete closure or prevent loop C capping (Hansen et al., 2005; Hibbs et al., 2009; Brams et al., 2011).

Our previous MD simulations of Y674-R685 bound to the α7 nAChR identified the guanidinium group of R682 in the SARS-COV-2 S protein as the key anchoring point to the α7 nAChR (Fig. 1C), forming strong interactions with several residues lining the receptor's ligand binding pocket (Oliveira et al., 2021). These simulations also show that, when bound to α7, the Y674-R685 region of the SARS-CoV-2 S protein adopts many different conformations within the binding pocket, ranging from highly compact to fully extended configurations (Supplementary Fig. 4). Some of these binding modes allow for the formation of the key interactions necessary to activate the receptor (Fig. 1C), while others do not (Supplementary Fig. 5) (Oliveira et al., 2021). Although the α7 nAChR has five identical orthosteric binding sites, agonist occupancy of only one is required to elicit channel activation (Andersen et al., 2013). Thus, it could be possible that the Y674-R685 fragment occupancy of the binding sites in multiple orientations, some of which cannot trigger activation, may contribute to its low efficacy, as described before for partial agonists (Hibbs et al., 2009). Alternatively, the partial closure of loop C in the presence of the Y674-R685 (Oliveira

et al., 2021) observed in some of our previous simulations may also reduce the efficacy for channel opening (Supplementary Fig. 6).

As shown here for Y674-R685, several compounds of different structures have dual opposite effects on nAChRs, including α7, by acting as agonists and non-competitive antagonists (also called negative allosteric modulators, NAMs) (Pereira et al., 2002; Fabiani et al., 2018; Lasala et al., 2019). NAMs comprise a wide range of structurally different compounds that inhibit receptor function by binding to sites distinct to the orthosteric sites (allosteric) (Chatzidaki and Millar, 2015). These allosteric sites may be located in different receptor domains, including the extracellular (Spurny et al., 2015) and transmembrane domains (Young et al., 2008; daCosta et al., 2011). The site from which Y674-R685 exerts inhibition as well as the precise mechanism remains to be determined. Non-competitive inhibition of channel activity may occur through enhanced desensitization, impaired opening, destabilization of the open state, channel blockade. We discard open-channel block since it is improbable that this region enters into the pore and also, fast flickering, typical of fast open-channel blockers, was not observed (Neher and Steinbach, 1978). Future competitive binding assays as well as experiments with mutant receptors will be useful to clearly identify the binding sites.

Conclusions

Our results identify a functional interaction between the Y674-R685 region of the SARS-CoV-2 S protein and the α7 nAChR. The S fragment exerts a dual effect on α7 nAChR, acting as a low-efficacy agonist and a non-competitive antagonist. Although the S fragment can activate the receptor with very low efficacy, its predominant effect may be inhibitory since activation does not occur in the absence of PAMs. It has been shown that activation of α7 nAChR in the immune system protects from excessive production of pro-inflammatory cytokines (e.g., TNF-α) (Rosas-Ballina et al., 2008) and, therefore, impairment of this receptor results in an overproduction of cytokines and enhanced tissue damage (Parrish et al., 2008). Our finding raises the possibility that α7 nAChRs may be involved in the hyper-inflammatory response associated to COVID-19 and opens door for its further exploration.

Declarations

ORCID

Juan Facundo Chrestia. 0000-0002-5223-383X

Ana Sofía Oliveira. 0000-0001-8753-4950

Adrian J. Mulholland. 0000-0003-1015-4567

Timothy Gallagher. 0000-0002-3544-327X

Isabel Bermúdez. 0000-0001-7692-1509

Cecilia Bouzat. 0000-0003-0388-6129

Acknowledgements: We thank Dr. Franco Vizcarra (Oxford Brookes University) for helping with the whole-cell recordings.

Author Contributions: JFC, ASFO, AJM, TG, IB and CB designed the research; JFC, ASFO, IB and CB performed the research and analysed the data; CB, ASFO, AJM, TG, JFC and IB wrote, reviewed, and/or edited the paper.

Funding: This work was supported by grants from Universidad Nacional del Sur (PGI 24/B298) and Agencia Nacional de Promoción Científica y Tecnológica (PICT 2017-1170) to CB; Oxford Brookes University (REA-2020) to IB. AJM and ASFO thank EPSRC (grant number EP/M022609/1) and BBSRC (grant number BB/R016445/1) for support. We thank BrisSynBio, a BBSRC/EPSRC Synthetic Biology Research Centre (Grant Number:BB/L01386X/1), for funding ASFO and providing funds to purchase the Y674-R685 peptide from Designer Bioscience Ltd. (Cambridge UK).

Competing interests: The authors have no relevant financial or non-financial interests to disclose.

Authors Contributions:JFC, ASFO, AJM, TG, IB and CB designed the research; JFC, ASFO, IB and CB performed the research and analysed the data; CB, ASFO, AJM, TG, JFC and IB wrote, reviewed, and/or edited the paper.All authors read and approved the final manuscript.

Ethics approval:not applicable

Consent to participate: not applicable

Consent for publication*:* not applicable

Availability of data and material. The data that support the findings of this study are available within the article.

References

1. Andersen N, Corradi J, Sine SM, Bouzat C (2013) Stoichiometry for activation of neuronal α7 nicotinic receptors. Proc Natl Acad Sci USA 110(51):20819–20824. https://doi.org/10.1073/pnas.1315775110
2. Andersen ND, Nielsen BE, Corradi J et al (2016) Exploring the positive allosteric modulation of human α7 nicotinic receptors from a single-channel perspective. Neuropharmacology 107:189–200. https://doi.org/10.1016/j.neuropharm.2016.02.032
3. Bertrand D, Gopalakrishnan M (2007) Allosteric modulation of nicotinic acetylcholine receptors. Biochem Pharmacol 74(8):1155–1163. https://doi.org/10.1016/j.bcp.2007.07.011
4. Bouzat C, Bren N, Sine SM (1994) Structural basis of the different gating kinetics of fetal and adult nicotinic acetylcholine receptors. Neuron 13:1395–1402. https://doi.org/10.1016/0896-

6273(94)90424-3

5. Bouzat C, Bartos M, Corradi J, Sine SM (2008) The interface between extracellular and transmembrane domains of homomeric Cys-loop receptors governs open-channel lifetime and rate of desensitization. J neuroscience: official J Soc Neurosci 28(31):7808–7819. https://doi.org/10.1523/JNEUROSCI.0448-08.2008
6. Bouzat C, Lasala M, Nielsen BE, Corradi J, Esandi M (2018) Molecular function of α7 nicotinic receptors as drug targets. J Physiol 596(10):1847–1861. https://doi.org/10.1113/JP275101
7. Brams M, Gay EA, Sáez JC et al (2011) Crystal structures of a cysteine-modified mutant in loop D of acetylcholine-binding protein. J Biol Chem 286(6):4420–4428. https://doi.org/10.1074/jbc.M110.188730
8. Cantuti-Castelvetri L, Ojha R, Pedro LD et al (2020) Neuropilin-1 facilitates SARS-CoV-2 cell entry and infectivity. Science 370(6518):856–860. https://doi.org/10.1126/science.abd2985
9. Casalino L, Gaieb Z, Goldsmith JA et al (2020) Beyond shielding: the roles of glycans in the SARS-CoV-2 spike protein. ACS Cent Sci 6:1722–1734. https://doi.org/10.1021/acscentsci.0c01056
10. Changeux JP, Taly A (2008) Nicotinic receptors, allosteric proteins and medicine. Trends Mol Med 14(3):93–102. https://doi.org/10.1016/j.molmed.2008.01.001
11. Changeux JP, Amoura Z, Rey FA, Miyara M (2020) A nicotinic hypothesis for Covid-19 with preventive and therapeutic implications. CR Biol 343(1):33–39. https://doi.org/10.5802/crbiol.8
12. Chatzidaki A, Millar NS (2015) Allosteric modulation of nicotinic acetylcholine receptors. Biochem Pharmacol 97(4):408–417. https://doi.org/10.1016/j.bcp.2015.07.028
13. Chrestia JF, Bruzzone A, Esandi M, Bouzat C (2021) Tyrosine phosphorylation differentially fine-tunes ionotropic and metabotropic responses of human α7 nicotinic acetylcholine receptor. Cell Mol Life Sci 78(13):5381–5395. https://doi.org/10.1007/s00018-021-03853-3
14. daCosta CJ, Free CR, Corradi J, Bouzat C, Sine SM (2011) Single-channel and structural foundations of neuronal α7 acetylcholine receptor potentiation. J neuroscience: official J Soc Neurosci 31(39):13870–13879. https://doi.org/10.1523/JNEUROSCI.2652-11.2011
15. Daly JL, Simonetti B, Klein K et al (2020) Neuropilin-1 is a host factor for SARS-CoV-2 infection. Science 370(6518):861–865. https://doi.org/10.1126/science.abd3072
16. Dineley KT, Pandya AA, Yakel JL (2015) Nicotinic ACh receptors as therapeutic targets in CNS disorders. Trends in pharmacological sciences 36(2) 96–108 (2015). https://doi.org/10.1016/j.tips.2014.12.002
17. Egea J, Buendia I, Parada E et al (2015) Anti-inflammatory role of microglial alpha7 nAChRs and its role in neuroprotection. Biochem Pharmacol 97(4):463–472. https://doi.org/10.1016/j.bcp.2015.07.032
18. Fabiani C, Murray AP, Corradi J, Antollini SS (2018) A novel pharmacological activity of caffeine in the cholinergic system. Neuropharmacology 135:464–473. https://doi.org/10.1016/j.neuropharm.2018.03.041

19. Farsalinos K, Eliopoulos E, Leonidas DD et al (2020) Nicotinic Cholinergic System and COVID-19: In Silico Identification of an Interaction between SARS-CoV-2 and Nicotinic Receptors with Potential Therapeutic Targeting Implications. Int J Mol Sci 21(16):5807. https://doi.org/10.3390/ijms21165807
20. Fucile S (2004) Ca2 + permeability of nicotinic acetylcholine receptors. Cell Calcium 35(1):1–8. https://doi.org/10.1016/j.ceca.2003.08.006
21. Grant SN, Lester H (2021) Regulation of epithelial sodium channel activity by SARS-CoV-1 and SARS-CoV-2 proteins. Biophys J 120(14):2805–2813. https://doi.org/10.1016/j.bpj.2021.06.005
22. Grønlien JH, Håkerud M, Ween H et al (2007) Distinct profiles of alpha7 nAChR positive allosteric modulation revealed by structurally diverse chemotypes. Mol Pharmacol 72(3):715–724. https://doi.org/10.1124/mol.107.035410
23. Gu S, Matta JA, Lord B et al (2016) Brain α7 Nicotinic Acetylcholine Receptor Assembly Requires NACHO. Neuron 89(5):948–955. https://doi.org/10.1016/j.neuron.2016.01.018
24. Hoffmann M, Kleine-Weber H, Schroeder S et al (2020) SARS-CoV-2 Cell Entry Depends on ACE2 and TMPRSS2 and Is Blocked by a Clinically Proven Protease Inhibitor. Cell 181(2):271–280e8. https://doi.org/10.1016/j.cell.2020.02.052
25. Guan YZ, Jin XD, Guan LX et al (2015) Nicotine inhibits microglial proliferation and is neuroprotective in global ischemia rats. Mol Neurobiol 51(3):1480–1488. https://doi.org/10.1007/s12035-014-8825-3
26. Hansen SB, Sulzenbacher G, Huxford T et al (2005) Structures of Aplysia AChBP complexes with nicotinic agonists and antagonists reveal distinctive binding interfaces and conformations. EMBO J 24(20):3635–3646. https://doi.org/10.1038/sj.emboj.7600828
27. Hibbs RE, Sulzenbacher G, Shi J et al (2009) Structural determinants for interaction of partial agonists with acetylcholine binding protein and neuronal alpha7 nicotinic acetylcholine receptor. EMBO J 28(19):3040–3051. https://doi.org/10.1038/emboj.2009.227
28. Hueffer K, Khatri S, Rideout S et al (2017) Rabies virus modifies host behaviour through a snake-toxin like region of its glycoprotein that inhibits neurotransmitter receptors in the CNS. Sci Rep 7(1):12818. https://doi.org/10.1038/s41598-017-12726-4
29. Hurst RS, Hajós M, Raggenbass M et al (2005) A novel positive allosteric modulator of the alpha7 neuronal nicotinic acetylcholine receptor: in vitro and in vivo characterization. J neuroscience: official J Soc Neurosci 25(17):4396–4405. https://doi.org/10.1523/JNEUROSCI.5269-04.2005
30. Kabbani N, Nordman JC, Corgiat BA et al (2013) Are nicotinic acetylcholine receptors coupled to G proteins? BioEssays: news and reviews in molecular. Cell Dev biology 35(12):1025–1034. https://doi.org/10.1002/bies.201300082
31. Lansdell SJ, Gee VJ, Harkness PC et al (2005) RIC-3 enhances functional expression of multiple nicotinic acetylcholine receptor subtypes in mammalian cells. Mol Pharmacol 68(5):1431–1438. https://doi.org/10.1124/mol.105.017459

32. Lasala M, Fabiani C, Corradi J, Antollini S, Bouzat C (2019) Molecular Modulation of Human α7 Nicotinic Receptor by Amyloid-β Peptides. Front Cell Neurosci 13:37. https://doi.org/10.3389/fncel.2019.00037
33. Minguez-Viñas T, Nielsen BE, Shoemark DK et al (2021) A conserved arginine with non-conserved function is a key determinant of agonist selectivity in α7 nicotinic ACh receptors. Br J Pharmacol 178(7):1651–1668. https://doi.org/10.1111/bph.15389
34. Mukhtasimova N, Lee WY, Wang HL, Sine SM (2009) Detection and trapping of intermediate states priming nicotinic receptor channel opening. Nature 459:451–454. https://doi.org/10.1038/nature07923
35. Nau J, Luthra P, Lanzer K et al (2021) Varenicline prevents SARS-CoV-2 infection in vitro and in Rhesus Macaques. https://doi.org/10.1101/2021.06.29.450426. accessed 20 September 2021) bioRxiv [Preprint]
36. Neher E, Steinbach JH (1978) Local anaesthetics transiently block currents through single acetylcholine-receptor channels. J Physiol 277:153–176. https://doi.org/10.1113/jphysiol.1978.sp012267
37. Nielsen BE, Minguez T, Bermudez I, Bouzat C (2018) Molecular function of the novel α7β2 nicotinic receptor. Cell Mol Life Sci 75(13):2457–2471. https://doi.org/10.1007/s00018-017-2741-4
38. Nielsen E, Bermudez I, Bouzat C (2019) Flavonoids as positive allosteric modulators of α7 nicotinic receptors. https://doi.org/10.1016/j.neuropharm.2019.107794. Neuropharmacology 160 107794
39. Noviello CM, Gharpure A, Mukhtasimova N et al (2021) Structure and gating mechanism of the α7 nicotinic acetylcholine receptor. Cell 184(8):2121–2134e13. https://doi.org/10.1016/j.cell.2021.02.049
40. Oliveira A, Ibarra AA, Bermudez I et al (2021) A potential interaction between the SARS-CoV-2 spike protein and nicotinic acetylcholine receptors. Biophys J 120(6):983–993. https://doi.org/10.1016/j.bpj.2021.01.037
41. Parrish WR, Rosas-Ballina M, Gallowitsch-Puerta M et al (2008) Modulation of TNF release by choline requires alpha7 subunit nicotinic acetylcholine receptor-mediated signaling. Mol Med 14(9–10):567–574. https://doi.org/10.2119/2008-00079.Parrish
42. Pereira EF, Hilmas C, Santos MD et al (2002) Unconventional ligands and modulators of nicotinic receptors. J Neurobiol 53(4):479–500. https://doi.org/10.1002/neu.10146
43. Pinheiro NM, Santana FP, Almeida RR et al (2017) Acute lung injury is reduced by the α7nAChR agonist PNU-282987 through changes in the macrophage profile. FASEB journal: official publication of the Federation of American Societies for Experimental Biology 31(1):320–332. https://doi.org/10.1096/fj.201600431R
44. Rosas-Ballina M, Ochani M, Parrish WR et al (2008) Splenic nerve is required for cholinergic antiinflammatory pathway control of TNF in endotoxemia. Proc Natl Acad Sci USA 105(31):11008–11013. https://doi.org/10.1073/pnas.0803237105

45. Russo P, Bonassi S, Giacconi R et al (2020) COVID-19 and smoking: is nicotine the hidden link? Eur Respir J 55(6):2001116. https://doi.org/10.1183/13993003.01116-2020
46. Spurny R, Debaveye S, Farinha A et al (2015) Molecular blueprint of allosteric binding sites in a homologue of the agonist-binding domain of the α7 nicotinic acetylcholine receptor. Proc Natl Acad Sci USA 112(19):E2543–E2552. https://doi.org/10.1073/pnas.1418289112
47. Uteshev V (2014) The therapeutic promise of positive allosteric modulation of nicotinic receptors. Eur J Pharmacol 727:181–185. https://doi.org/10.1016/j.ejphar.2014.01.072
48. Wang H, Yu M, Ochani M et al (2003) Nicotinic acetylcholine receptor alpha7 subunit is an essential regulator of inflammation. Nature 421(6921):384–388. https://doi.org/10.1038/nature01339
49. Wonnacott S (2014) Nicotinic ACh Receptors.Tocris Bioscience Scientific Reviews Series1–31
50. Yan R, Zhang Y, Li Y et al (2020) Structural basis for the recognition of SARS-CoV-2 by full-length human ACE2. Science 367(6485):1444–1448. https://doi.org/10.1126/science.abb2762
51. Yang T, Xiao T, Sun Q, Wang K (2017) The current agonists and positive allosteric modulators of α7 nAChR for CNS indications in clinical trials. Acta Pharm Sinica B 7(6):611–622. https://doi.org/10.1016/j.apsb.2017.09.001
52. Young GT, Zwart R, Walker AS, Sher E, Millar NS (2008) Potentiation of alpha7 nicotinic acetylcholine receptors via an allosteric transmembrane site. Proc Natl Acad Sci USA 105(38):14686–14691. https://doi.org/10.1073/pnas.0804372105
53. Zwart R, De Filippi G, Broad LM et al (2002) 5-Hydroxyindole potentiates human alpha 7 nicotinic receptor-mediated responses and enhances acetylcholine-induced glutamate release in cerebellar slices. Neuropharmacology 43(3):374–384. https://doi.org/10.1016/s0028-3908(02)00094-1

Figures

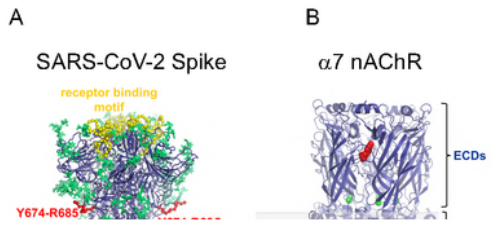

Figure 1

Three-dimensional structures of the SARS-CoV-2 S protein and the human α7 nAChR.

A. The model represents the complete, fully glycosylated S protein in the closed state after furin cleavage (Casalino et al., 2020). The protein is rendered as a blue cartoon with the glycans depicted in green. The receptor binding motifs (residues S438-Q506) and the Y674-R685 region are highlighted in yellow and

red, respectively. The Y674-R685 region was shown to be accessible for binding in previous MD simulations of the fully glycosylated S protein (Oliveira et al., 2021).

B. Cryo-EM structure of the human α7 nAChR (PDB code: 7KOX) (Noviello et al., 2021). This receptor is a homopentamer formed of five α7 subunits. Each subunit is composed of an extracellular (ECD), transmembrane (TMD) and intracellular (ICD) domain. The agonist binding site is located in the ECD at the interface between two neighbouring subunits. In this structure, epibatidine (red spheres) is bound to the agonist binding site. The green spheres represent bound calcium ions.

C. MD simulations of Y674-R685 bound to the human α7 nAChR show favourable binding to the binding pocket (Oliveira et al., 2021). Example of conformations from simulations in which the most important interactions with conserved key aromatic residues are present. Left: Overall view of the Y674-R685: α7(ECD) complex. Right: Close-up view of interactions formed by R682 and Q675 within agonist binding site. The α7 receptor and Y674-R685 are coloured in dark blue and orange, respectively. Interactions between side chains of R682 and Q675 and the aromatic rings of TrpB ((α7W171), TyrC1 (α7Y210), TyrC2 (α7Y217) and TyrA (α7Y115) are shown with dashed lines.

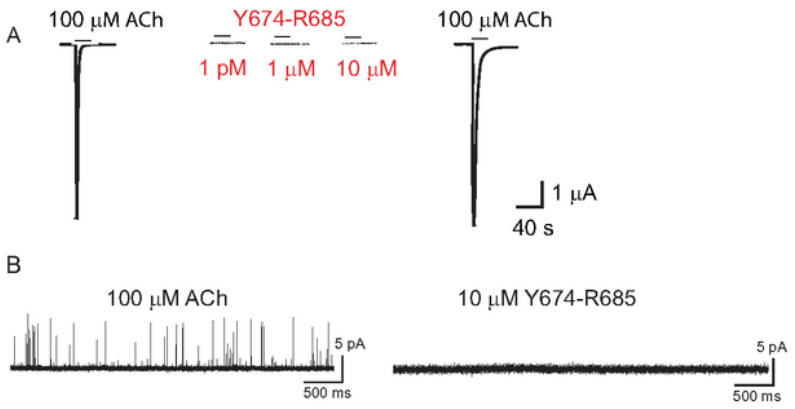

Figure 2

The Y674-R685 fragment cannot elicit detectable α7 responses.

A. Macroscopic responses of the human α7 nAChR. Representative traces from single oocytes expressing human α7 nAChR to applications of ACh (100 μM) or 1 pM, 1 mM or 10 mM of Y674-R685. Drug applications were for 20 s followed by a 300 s washout.

B. Single-channel currents of the human α7 nAChR recorded from cell-attached patches in the presence of 100 μM ACh or 10 μM Y674-R685. No channel activity was detected at a 1 pM-100 μM Y674-R685 concentration range. Channel openings are shown as upward deflections. Membrane potential: -70 mV. Filter: 9 kHz.

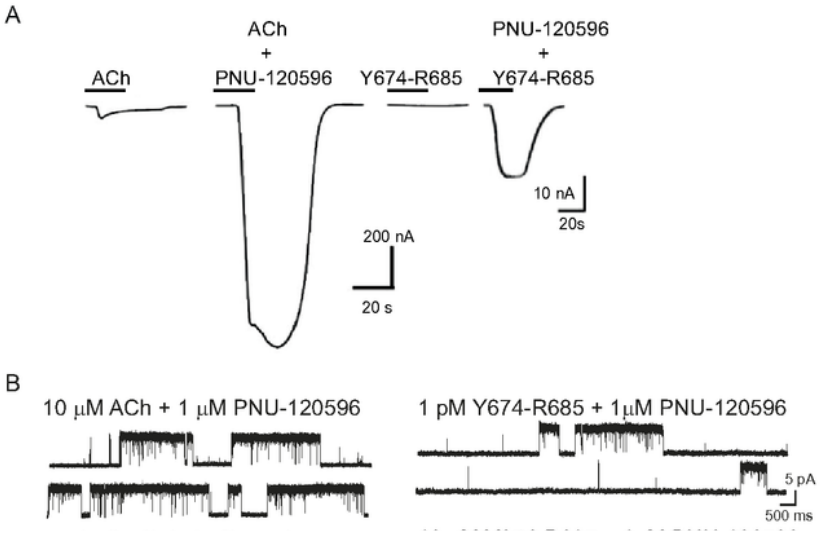

Figure 3

Activation of the human α7 nAChR by Y674-R685 in the presence of the PAM PNU-120596.

A. Macroscopic currents were recorded from oocytes expressing the human α7 nAChR after a pulse of 30 µM ACh (control) or 1 µM Y674-R685 in the absence or presence of 10 µM PNU-120596. Current traces shown are representative of n=15 recordings from oocytes isolated from N=3 donors.

B. Single-channel currents of the human α7 nAChR in the presence of the type II PAM PNU-120596 (1 µM) activated by 100 µM ACh (left), or Y674-R685 at 1 pM or 10 µM (right). For each condition typical channel traces are shown. Channel openings are shown as upward deflections. Membrane potential: -70 mV. Filter: 3 kHz.

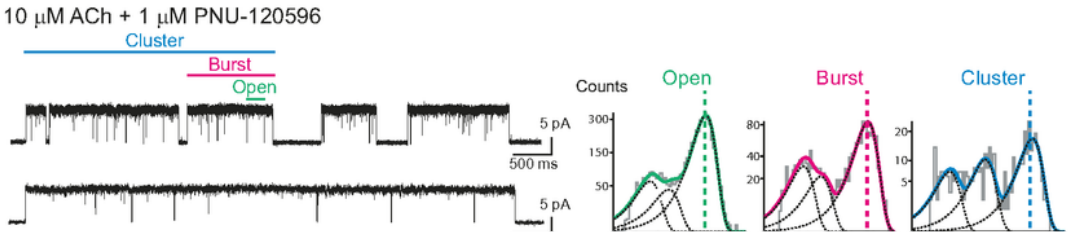

Figure 4

Single-channel recordings of the human α7 nAChR in the presence of Y674-R685.

Single-channel currents of human α7 nAChR in the presence of the type II PAM PNU-120596 (1μM) activated by 100 μM ACh, or Y674-R685 at 1 pM or 10 μM. For each condition, channel traces at two different temporal scales are shown. Channel openings are shown as upward deflections. Representative

open, burst and cluster duration histograms are shown for each condition. The open, burst and cluster durations correspond to the durations of the slowest components of each histogram. The dashed lines show how these mean durations change among different conditions. Membrane potential: -70 mV. Filter: 3 kHz.

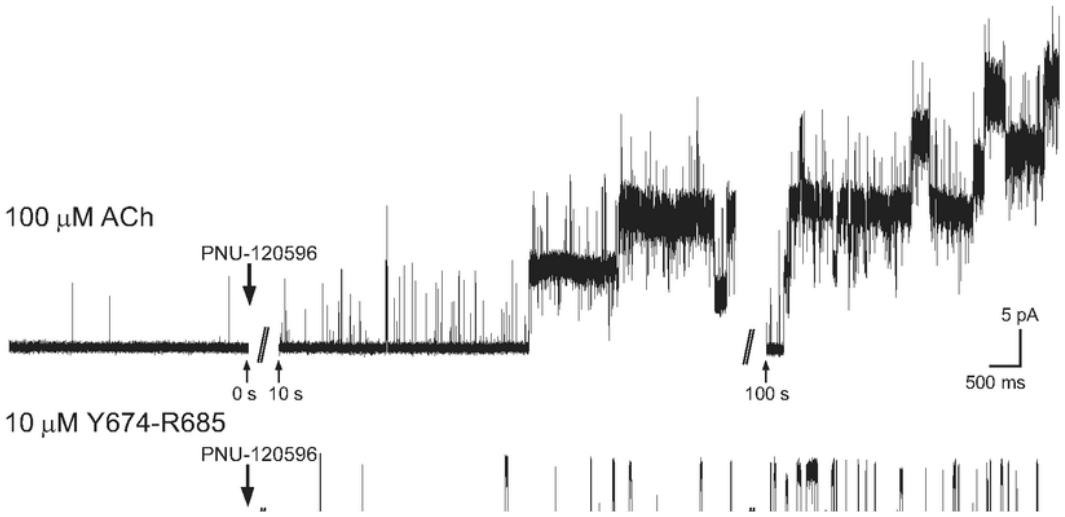

Figure 5

Channel activity elicited by Y674-R685 in the absence or presence of the PAM.

Representative experiments in which channel activity from the same patch was recorded before and after addition of PNU-120596. ACh or 10 μM Y674-R685 were present in the pipette solution.

The indicated time corresponds to the time of recording after addition of PNU-120596.

Top: Single-channel currents of human α7 activated by 100 μM ACh appeared mainly as brief isolated openings. Addition of 1 μM PNU-120596 to the extracellular solution surrounding a cell-attached patch resulted in a marked increase in current in the continued presence of 100 μM ACh in the patch pipette. This experiment is representative of 4 different patches.

Bottom: Channel activity was undetectable in the presence of Y674-R685. Addition of 1 μM PNU-120596 to the extracellular solution surrounding the silent patch revealed channel activity, indicating that only in the presence of the PAM 10 μM Y674-R685 can activate α7. This experiment is representative of 3 different patches.

Channel openings are shown as upward deflections. Membrane potential: -70 mV. Filter 3 kHz.

Figure 6

Activation of the human α7 nAChR by Y674-R685 in the presence of the type I PAM, 5-HI.

Single-channel currents were recorded from cells expressing the human α7 nAChR in the presence of 2 mM 5-HI as the PAM and 100 μM ACh or 10 μM Y674-R685 as agonists. Traces at two different scales are shown for each condition. Membrane potential: -70 mV, Filter: 9 kHz. Representative open and burst duration histograms are shown for each agonist. The bar chart shows the mean durations of open and bursts for each agonist (n=37 for ACh, and n=3 for Y674-R685). *$p<0.05$, **$p<0.01$.

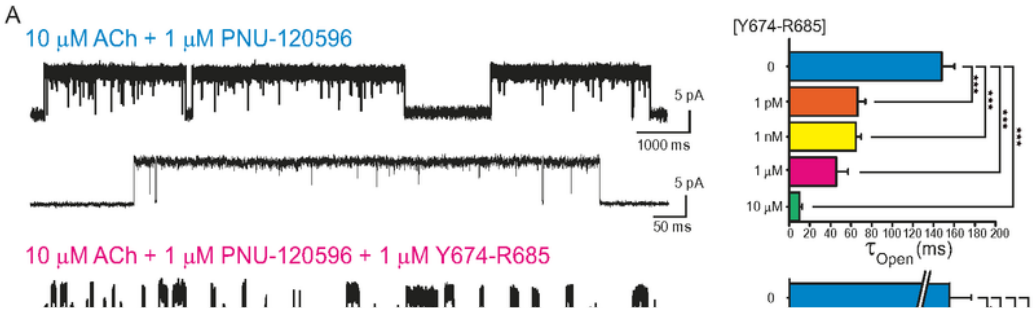

Figure 7

Y674-R685 Inhibition of α7 nAChR channels activated by ACh.

A. Single-channel currents elicited by 10 μM ACh and potentiated by 1 μM PNU-120596 were recorded in the absence (control) or presence of 1 or 10 μM Y674-R685.

Left: Typical channel traces are shown at two different temporal scales. Channel openings are shown as upward deflections. Membrane potential: -70 mV. Filter: 3 kHz.

Right: Bar chart showing the mean durations of openings (topen), bursts (tburst) and clusters (tcluster) in the absence and in the presence of 1 pM, 1 nM, 1 μM and 10 μM Y674-R685.

**p<0.01, *** p<0.001 (Student-t Test) (Supplementary Table 1).

B. Left Panel: Concentration response curve (CRC) for the inhibition of the α7 nAChR by Y674-R685**.** Increasing concentrations of Y674-R685 (0.1 nM to 30 μM) were co-applied with control ACh (100 μM). Responses were measured fom the peak of ACh-elicited currents. Each data point represents the average normalized response of six cells (± SEM).

Right Panel: Competition CRC data (red) for 1 μM Y674-R685 co-applied with different ACh concentrations (0.1-2000 μM). For comparison, ACh CRC data alone (black) are shown at the same concentrations. Data were fitted with the Hill equation, as described in Methods. Data points represent the average normalized response of six oocytes (± SEM).

Supplementary Files

This is a list of supplementary files associated with this preprint. Click to download.

- SupportingInformationChrestiaetalMN2022.pdf